Task 3: Corrosion Tests at 500°C

High temperature autoclave testing was performed at 500°C to assess the feasibility of utilizing Zr-based alloys in supercritical water (SCW) applications. The high temperature test environments included 500°C/1500 psi steam and 500°C/3650 psi supercritical water (SCW). Testing was performed in a manner consistent with the ASTM G2. The corrosion behavior of the specimens was evaluated by measuring the weight gain as a function of the exposure time.

The corrosion test in supercritical water was performed in two types of facilities: (i) a static autoclave (closed environment in which water does not recirculate) at KAERI (designated as SCW static) and (ii) a dynamic loop system (water is constantly refreshed, and chemistry is controlled) at the University of Michigan (designated as SCW dynamic). Details of the testing at the University of Michigan are described below. The 500°C steam corrosion test was performed at Westinghouse and KAERI in static autoclaves at 10.3 MPa (1500 psi). Corrosion coupons for all testing at 500°C were comparable to those prepared for testing in 360°C environments. Coupon size was 20 mm × 25 mm and the surface was prepared by mechanical grinding following by pickling and thorough rinsing.

A test environment of 500°C is very aggressive for Zr-based alloys as prior experience has shown that widely used alloy such as Zircaloy-4 forms very thick oxide films after a few days of exposure in 500°C steam. The results from testing of the model alloys in this program have demonstrated that some of the compositions exhibit significant improvement over Zircaloy-4. Sample weight gains for the model alloys are provided in the appendices (Appendix C). The results of the testing are discussed below following a description of the supercritical water test facility at the University of Michigan.

Corrosion Testing at 500°C Supercritical Water Test Facility (University of Michigan)

All corrosion tests at the University of Michigan were conducted in a flowing supercritical water loop (Figure 3.1). The closed loop system operated at a flow rate of 12 ml/min. Water in a main column is continually pumped through a secondary loop where impurities are filtered out by an ion exchanger. A gas line feeds into the bottom of the main column, in which Ar gas is bubbled to deoxygenate the water to <10 ppb O_2.

The main loop of the system consisted of a pump, pre-heater, autoclave, chiller, and back-pressure regulator (BPR). Water flowed from the bottom of the main column into a high pressure liquid chromatography pump capable of flow rates to 100 ml/min and rated to 6000 psi at 24 ml/ min. The water was pumped into a pre-heater, which raised the temperature of the water from room temperature to approximately 440°C. Water from the pre-heater passed through an insulated section of pipe into the autoclave (Figure 3.2). Water entered the autoclave at the bottom of the enclosure; the entrance of the outlet line was located at the top. As the autoclave filled, the corrosion coupons were immersed in water that was eventually forced out the top when the autoclave was full. The autoclave was heated by three heater bands, which brought the temperature up to

500°C. They were positioned so that temperature within the autoclave remained uniform and stable. After exiting the autoclave, water passed through a chiller where heat was exchanged with an external line of flowing cold water to bring the water temperature down to room temperature. Pressure in the autoclave was controlled by a BPR rated to 4000 psi on the outlet line. Low-pressure water on the backside of the BPR was passed through another ion exchanger and back into the top of the main column. All high-temperature areas of the loop were enclosed in a 2.54 cm thick Lexan shield to protect lab personnel and equipment from any steam leaks that could occur.

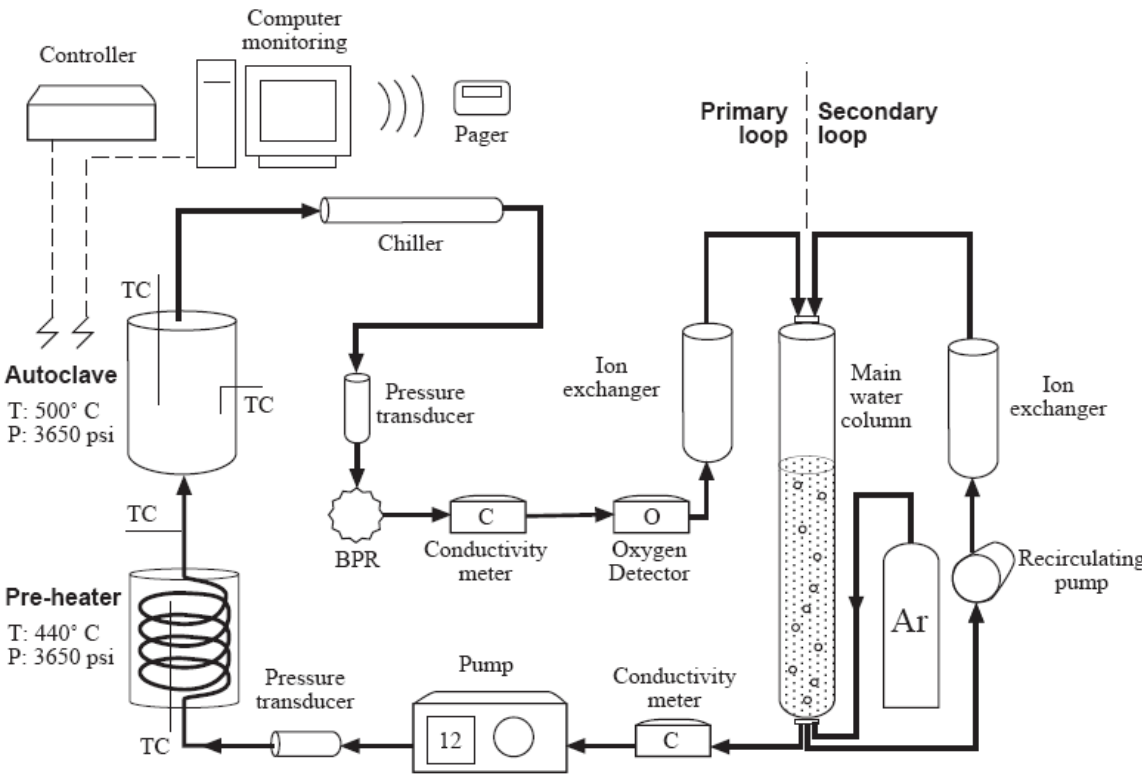

Figure 3.1: Schematic of the flowing supercritical water loop.

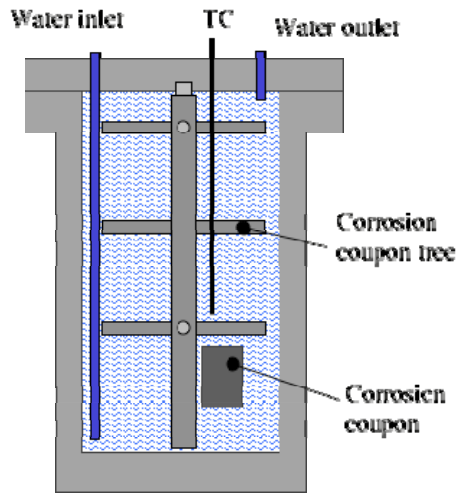

Figure 3.2: A diagram of the inside of the autoclave.

Corrosion coupons were hung from an internal tree by Inconel wire that hooked through the hole in each coupon and wrapped around a branch of the tree. The tree was capable of supporting up to 48 samples at a time, allowing each sample to be exposed on all surfaces except the small area within the hole touched by the wire. Two coupons of each alloy were tested simultaneously in all corrosion tests to increase the reliability of the results. Coupons of the same alloy were hung on opposite sides of the autoclave to detect any lack of uniformity in internal autoclave conditions.

Conductivity, temperature, oxygen content and pressure in the loop were measured throughout the test. Conductivity was measured in the inlet line between the main column and pump, and again in the outlet line immediately after the BPR. The ion exchange system maintained the conductivity of the inlet water at values as low as 0.06µS/cm. The temperature was measured by thermocouples located in the center of the pre-heater coils, at the inlet line, attached to the external side of the autoclave, and close to the center of the inside of the autoclave. The inlet and internal thermocouples were used primarily to monitor and record the temperatures of water entering and within the autoclave. The thermocouples in the pre-heater and on the outside of the autoclave were used by temperature controllers located next to the system. These controllers regulated the current to the pre-heater and heater bands using solid state relays. The constant feedback the controllers received from the thermocouples allowed both heating systems to be maintained at stable temperatures throughout the test, and were crucial for increasing and decreasing temperature at system startup and shutdown. Dissolved oxygen content was measured by an Orbisphere Model 2713 High Sensitivity Oxygen Detector that can analyze water from either the inlet or outlet line. Two Omega pressure transducers measured pressure at the inlet to the pre-heater and on the high-pressure side of the BPR. The temperature, pressure, and conductivity data were relayed to a computer running LabView software that records new data every 10 seconds. To help ensure safety and system stability, LabView can also contact lab personnel through pagers when system parameters exceed set bounds.

The tests were conducted in accordance with the standards described in ASTM G2-88. Argon was bubbled through the main column until the dissolved oxygen content was less than 10 ppb. The loop was run in bypass mode until initial conductivity of the water was as low as possible, typically around 0.06µS/cm. The autoclave was then purged with argon and filled with water. The autoclave was pressurized to approximately 25.1 MPa (3650 psi) using the BPR and heated to 500°C. After each test ran for a specified amount of time, the autoclave temperature was lowered to room temperature and pressure, and subsequently drained and opened. Shortly after being recovered from the autoclave, the corrosion coupon surfaces were photographed with a digital camera to record their appearance.

500℃ Corrosion Results

The high temperature corrosion testing of the model alloys was performed in 500°C steam and in 500°C supercritical water. The alloys tested in 500°C were the same as those tested in 360°C water. Results from the multiple test facilities and test environments revealed common trends in the performance of the model alloys. Details of the weight gain measurements are provided in the appendices with the results summarized in Table 3.1.

It is apparent that alloys with no precipitate-forming alloy additions exhibit the poorest behavior at elevated temperature. These include the Zr-Sn alloys, Zr-0.2Nb, Zr-Sn-Nb alloys, and Zr (sponge and crystal bar). These alloys did not survive the high temperature for even short term exposures. Also included in this group of alloys is Zircaloy-4 which contains the solute Sn as well as small additions of precipitate-forming elements Fe and Cr. These alloys (solute alloys plus Zircaloy-4) are the first ten listed in Table 3.1.

Figure 3.3 shows results from Zr-Sn-Nb that exhibited breakaway and nodular corrosion behavior after relatively short exposure times. Zr-Sn binary alloys were very susceptible to corrosion in 500°C steam and in 500°C supercritical water. The corrosion weight gain increased to more than 2500mg/dm^2 just after 1 day in 500°C steam and the corroded specimen which was entirely covered with the white oxide was easily broken just by a small force when handle to measure the weight gain.

The remaining model alloys (with the possible exception of Zr-0.4Nb) are the alloys that form second phase particles (SPPs). (Note: Zr-0.4Nb likely contains SPPs due to the presence of iron impurities in the alloy). The corrosion weight gains measured for the Zr-Nb alloys are shown in Figure 3.4. The weight gains are similar for all of the alloys with more than 0.2 Nb, and the oxide appears to be protective for over 240 days in 500°C SCW, although with a reasonably high corrosion rate. The corrosion behavior of Zr-Nb alloys in 500°C steam and supercritical water was approximately the same. The exception to this group was the Zr-0.2Nb alloy which showed breakaway behavior and oxide spalling in the early stages of corrosion in both corrosion environments, showing a weight gain of 1793mg/dm^2 after 1 day and an oxide that was entirely white. Overall,

the corrosion rate of Zr-Nb alloys in supercritical water was twenty times higher than that in 360°C pure water. The results from KAERI are similar to those from the 500°C steam testing at Westinghouse with poor performance of Zr-0.2Nb and comparable behavior of the higher Nb-content alloys.

Figure 3.5 and Figure 3.6 show the corrosion behavior of Zr-Fe-Cr alloys in 500°C steam and supercritical water. Fe and Cr content were changed to vary the volume fraction of the precipitates. Zr-0.2Fe-0.1Cr and Zr-0.4Fe-0.2Cr alloys were processed at 580°C and 720°C to change the precipitate size. The higher alloy content Zr-0.4Fe-0.2Cr material performed consistently better in steam and SCW among the four test facilities (see Table 3.1). Some variability is noted as Zr-0.2Fe-0.1Fe showed comparable results in steam (KAERI) (Figure 3.5a) and SCW (UM) (Figure 3.6b). However, these alloys (Zr-0.2Fe-0.1Cr) performed poorly in steam (Westinghouse) and SCW (KAERI) after short times regardless of the processing temperature.

Corrosion results for Zr-Cr-Fe alloys are shown in Figure 3.7a (SCW – KAERI) and Figure 3.8 (steam – W, and SCW – UM). The beneficial effect of Fe is clear as seen by comparing the corrosion results of the binary Zr-Cr alloys and Zr-Cr-Fe (see Table 3.1). Zr-Fe-Cr ternary alloys showed better corrosion resistance than the binary Zr-Cr alloys, suggesting that Fe additions improved the corrosion resistance of Zr-Cr binary alloys. (It is possible that the comparable performance of Zr-1.0Cr in SCW (Figure 3.7a) is due to the presence of iron impurities in the material.)

Corrosion results from Zr-Cu-Mo alloys in SCW (KAERI) are shown in Figure 3.7b. These alloys were melted and rolled into strip in ROK. The binary Zr-Cu alloys showed protective behavior throughout the test but with weight gains somewhat higher than the Zr-Cr-Fe alloys. The higher Cu content alloy (Zr-1.0Cu) showed marginally better corrosion resistance than the Zr-0.5Cr alloy, in agreement with the general trend of higher alloying element content being beneficial to corrosion resistance at elevated temperatures. The presence of Mo had a deleterious impact on the corrosion resistance of the material, causing nodular corrosion and increasing the overall weight gain. The Zr-0.5Cu-0.5Mo oxide exhibited non-protective behavior from the start of the test while the Zr-1.0Cu-0.5Mo alloy showed protective behavior, but later developed nodular oxide and increased corrosion rate. Mo was also found to be detrimental to manufacturing the alloys when it was processed at 580°C as the Mo-containing alloys were susceptible to edge cracking of the strip during the cold rolling step. Results from Zr-Cu-Mo alloys that were fabricated in the US showed poorer corrosion behavior for both Zr-Cu and Zr-Cu-Mo (see Table 3.1).

Corrosion tests for the 2004 manufactured alloys (Table 1.2) were also performed in supercritical water. The additional alloys were designed to have a higher alloying content when compared to the original model alloys primarily because the results from the original model alloys indicated that precipitate-forming alloys with higher alloying content showed promise in improving the corrosion resistance in 500°C supercritical water. Results from the new model alloys are shown in Figure 3.9. The additional model alloys did not show better corrosion resistance than the best performing of the

original model alloys. However, all of the new precipitate-forming alloys exhibited better performance than the solute alloys confirming that the presence of precipitates is important in improving the high temperature corrosion performance. It is possible that there is an optimal composition to improve the corrosion resistance in 500°C supercritical water, or the lack of improvement for higher alloying contents could be related to the processing heat treatment.

Table 3.1: Summary of 500°C Corrosion Testing

Alloy	500°C Steam		500°C SCW	
	Westinghouse	KAERI	UM	KAERI
Zr-Sn Alloys				
Zr-0.2Sn	<1 day	1 day	-	1 day
Zr-0.4Sn	<1 day	1 day	-	1 day
Zr-0.8Sn	<1 day	1 day	-	1 day
Zr-1.2Sn	<1 day	1 day	-	1 day
Zr-0.2Nb Alloy				
Zr-0.2Nb	<1 day	1 day	-	1 day
Zr-Sn-Nb Alloys				
Zr-0.4Sn-0.2Nb	<1 day	30d (nodules)	-	6d
Zr-0.4Sn-0.2Nb	<1 day	30d (nodules)	-	6d
Reference Alloys				
Zr (sponge)	<1 day	-	-	1d (spall)
Zr (crystal bar)	<1 day	-	-	1d (spall)
Zircaloy-4	<1 day	-	1d (spall)	1d (2462)[1]
Zr-Nb Alloys				
Zr-0.4Nb	73d (528)[1]	30d (~350)[1]	-	240d (1487)[1]
Zr-1.0Nb	73d (495)[1]	30d (~350)[1]	-	240d (1496)[1]
Zr-1.5Nb	73d (538)[1]	30d (~350)[1]	-	240d (1434)[1]
Zr-2.5Nb	73d (552)[1]	30d (~350)[1]	-	240d (1420)[1]
Zr-Fe-Cr Alloys				
Zr-0.2Fe-0.1Cr L	<1 day	320d (~1100)[1]	-	3d (spall)
Zr-0.2Fe-0.1Cr H	<1 day	320d (~990)[1]	150d (211)[1]	3d (spall)
Zr-0.4Fe-0.2Cr L	129d (172)[1]	320d (~1200)[1]	150d (184)[1]	240d (771)[1]
Zr-0.4Fe-0.2Cr H	129d (340)[1]	320d (~1480)[1]	150d (306)[1]	240d (1220)[1]
Zr-Cr-Fe Alloys				
Zr-0.5Cr	<1 day	-	1d (4282)[1]	3d
Zr-0.5Cr-0.2Fe	76d (spall)	-	150d (204)[1]	240d (507)[1]
Zr-1.0Cr	4 d	-	-	240d (499)[1]
Zr-1.0Cr-0.2Fe	129d (222)[1]	-	150d (423)[1]	240d (344)[1]
Zr-Cu-Mo Alloys				
Zr-0.5Cu	<1 day	-	1d (3970)[1]	240d (700)[1]
Zr-0.5Cu-0.5Mo	<1 day	-	1d (spall)	3d (spall)
Zr-1.0Cu	32d (481)[1]	-	1d (550)[1]	240d (638)[1]
Zr-1.0Cu-0.5Mo	17d (221)[1]	-	1d (576)[1]	96 (spall)

[1] Number in parentheses is weight gain in mg/dm^2 at the specified time.

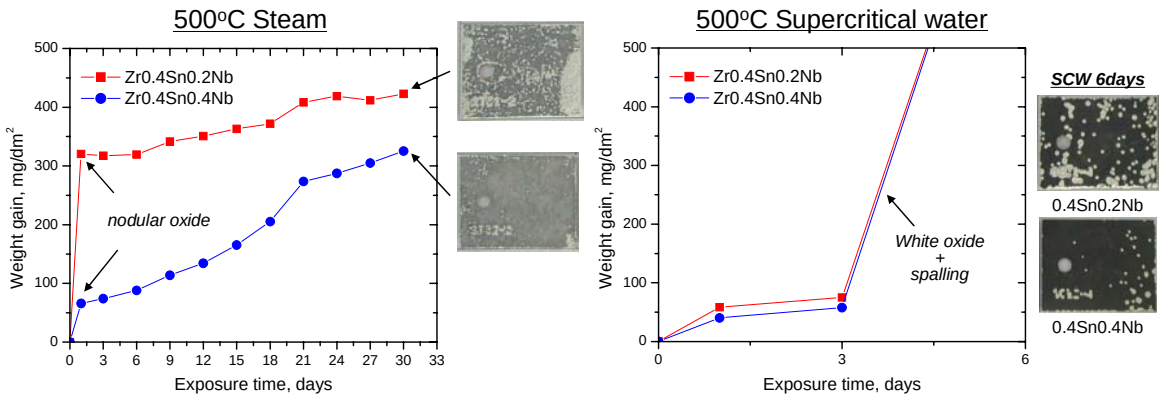

Figure 3.3: Corrosion behavior of Zr-Sn-Nb alloys in 500°C steam (KAERI) and supercritical water (KAERI).

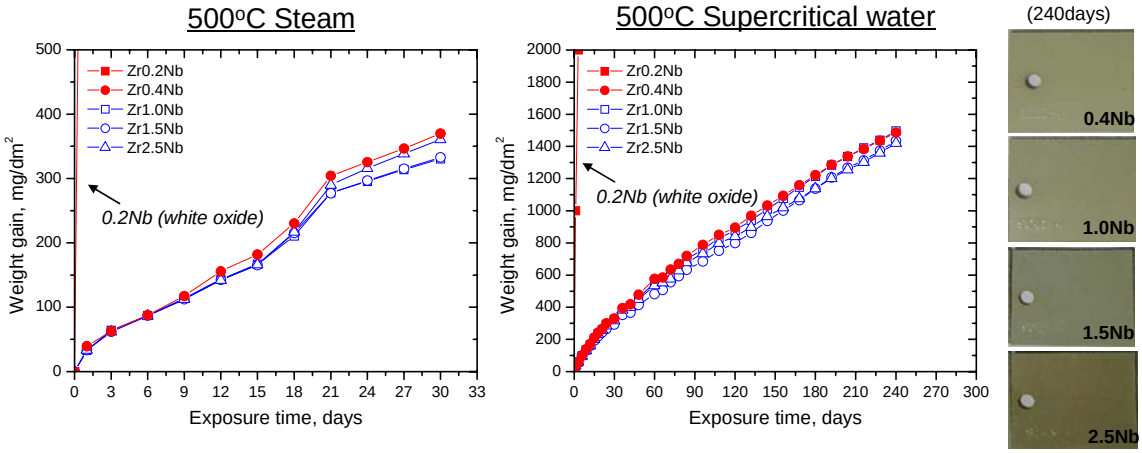

Figure 3.4: Corrosion behavior of Zr-Nb alloys in 500°C steam (KAERI) and supercritical water (KAERI).

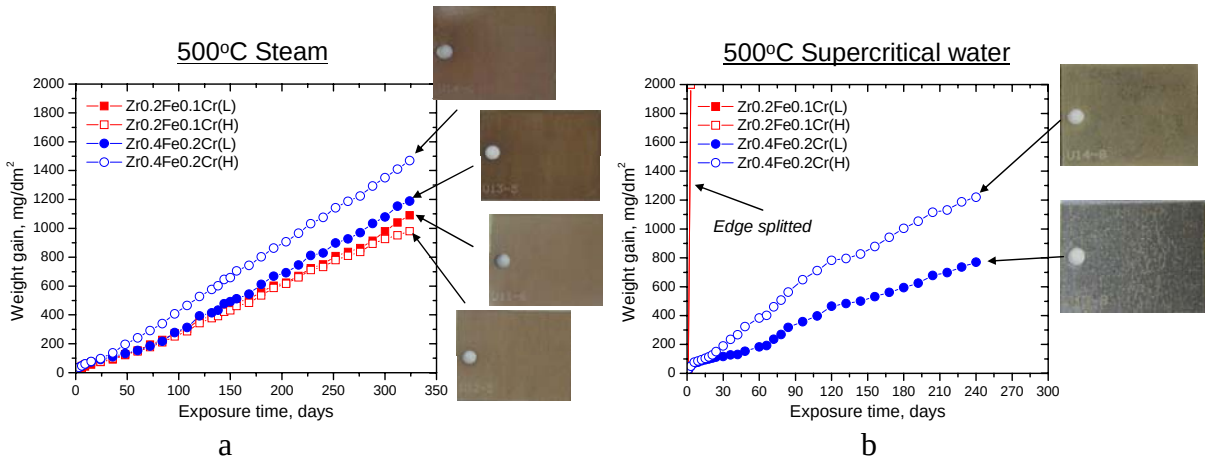

Figure 3.5: Corrosion behavior of Zr-Fe-Cr alloys in 500°C steam (KAERI) and supercritical water (KAERI).

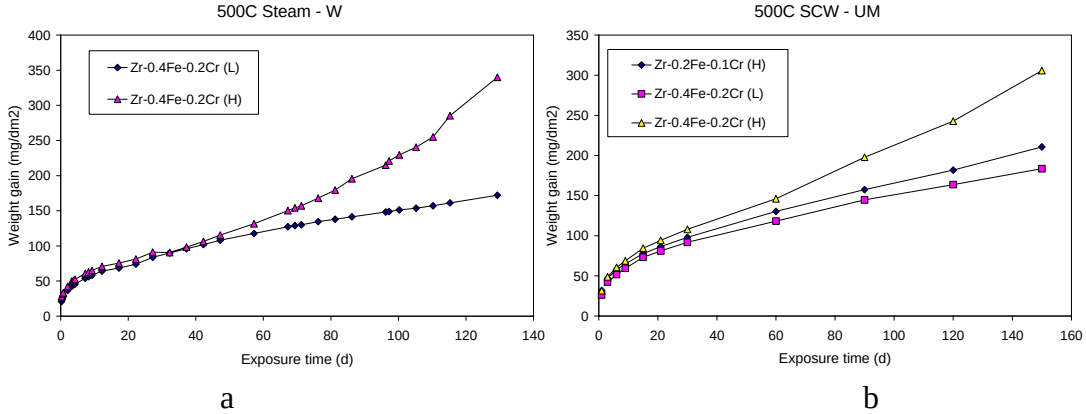

Figure 3.6: Corrosion behavior of Zr-Fe-Cr alloys in 500°C steam (W) and supercritical water (UM).

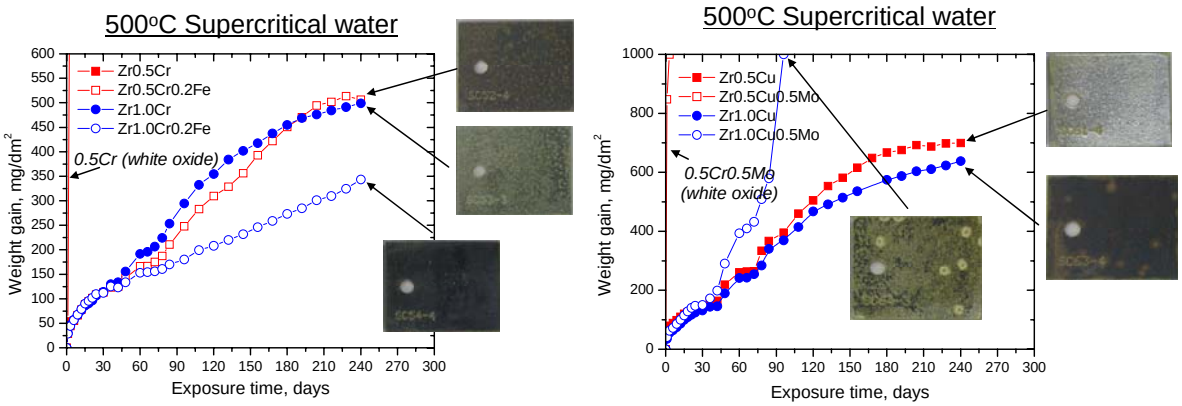

Figure 3.7: Corrosion behavior of Zr-Cr-Fe and Zr-Cu-Mo alloys in 500°C supercritical water (KAERI).

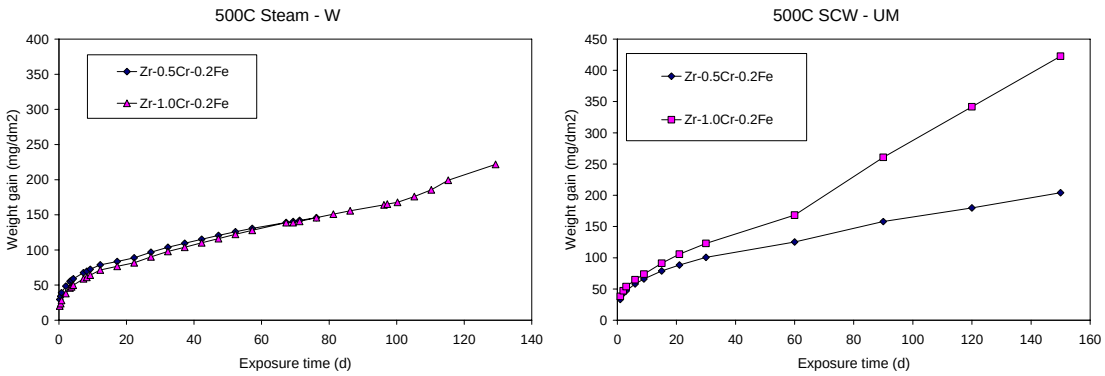

Figure 3.8: Corrosion behavior of Zr-Cr-Fe in 500°C steam (W) and supercritical water (UM).

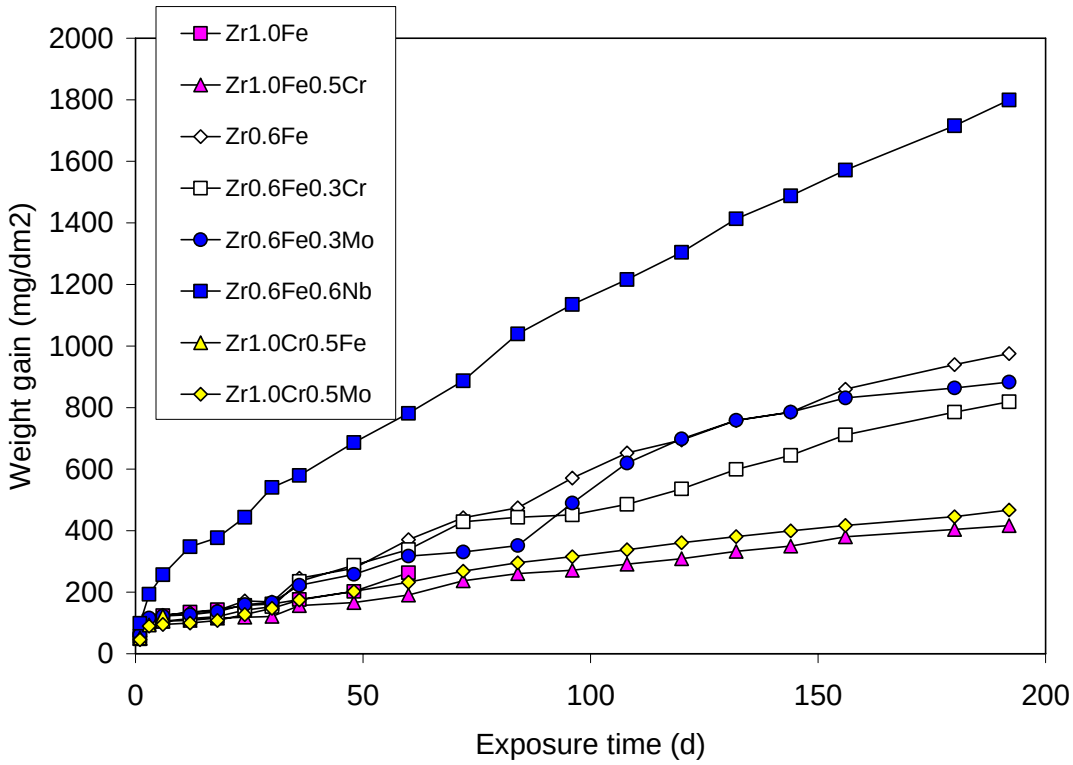

Figure 3.9: Corrosion behavior of new (precipitate-forming) model alloys in supercritical water (KAERI).

Pre-transition kinetic constants

Fitting of the kinetic curves was performed similar to that done at low temperature and the results are shown in Table 3.2. Not much difference is seen in the calculated values of A and n among the different environments for a given alloy. In general the values of A are much higher (30-35) than at 360 °C (which shows values of about 7-10). For the precipitate-based alloys the value of n is close to being cubic (n=0.33) and is somewhat higher than the values calculated at 360 °C, which were on the order of 0.2-0.25. In contrast the Zr-Nb alloys exhibit a considerably higher value of n, near 0.66. The ZrFeNb alloy shows an intermediate value of n, at 0.43. Similar tendencies were observed in the calculations of the values of n for low temperature corrosion of the same alloys, i.e., the lowest values of n were for the ZrFeCr and ZrCrFe alloys and the highest for the ZrNb alloys, with intermediate values for mixtures of the two. This suggests that the alloying elements have an effect on the atomic transport in the oxide layer, likely by affecting the concentrations of oxygen vacancies that are responsible for transport of oxidizing species through the layer.

Alloy	**Condition**	*A*	*n*	$\bar{n}$
Zr0.4Fe0.2Cr (L)	SCW dynamic	32	0.34	0.32
	500 ºC steam	31	0.29	
Zr-0.4Fe-0.2Cr (H)	SCW dynamic	32	0.36	
	500 ºC steam	38	0.25	
	SCW static	35	0.36	
Zr-1.0Cr-0.2Fe	SCW dynamic	36	0.35	0.33
	500 ºC steam	30	0.33	
	SCW static	30	0.30	
Zr-0.5Cr-0.2Fe	SCW dynamic	33	0.36	0.33
	500 ºC steam	40	0.30	
Zr0.6Fe	500 ºC steam	30	0.35	0.33
Zr0.6Fe0.3Cr		26	0.33	
Zr0.6Fe0.3Mo		38	0.30	
Zr1.0Fe	500 ºC steam	35	0.33	0.35
Zr1.0Fe0.5Cr		26	0.35	
Zr1.0Cr0.5Fe		24	0.35	
Zr1.0Cr0.5Mo		24	0.36	
Zr0.6Fe0.6Nb	500 ºC steam	32	0.43	0.43
Zr-0.4Nb	SCW static	30	0.71	0.67
Zr-1.0Nb		31	0.67	
Zr-1.5Nb		33	0.64	
Zr-2.5Nb		33	0.65	

Table 3.2: Calculated values of *A* and *n* for the initial protective stage of the corrosion process.